Diffusion-limited aggregation as a Markovian process: Site-sticking conditions

Boaz Kol and Amnon Aharony
Raymond and Beverly Sackler Faculty of Exact Sciences, School of Physics and Astronomy, Tel Aviv University, 69978 Ramat Aviv, Israel

(Received 20 September 2000; published 29 March 2001)

Cylindrical lattice diffusion-limited aggregation, with a narrow width N, is solved for site-sticking conditions using a Markovian matrix method (which was previously developed for the bond-sticking case). This matrix contains the probabilities that the front moves from one configuration to another at each growth step, calculated exactly by solving the Laplace equation and using the proper normalization. The method is applied for a series of approximations, which include only a finite number of rows near the front. The fractal dimensionality of the aggregate is extrapolated to a value near 1.68.

DOI: 10.1103/PhysRevE.63.046117 PACS number(s): 02.50.−r, 05.20.−y, 61.43.Hv

I. INTRODUCTION

Diffusion-limited aggregation (DLA) [1] has been the subject of extensive study since it was first introduced. This model exhibits a growth process that produces highly ramified self-similar patterns, which are believed to be fractals [2]. It seems that DLA captures the essential mechanism in many natural growth processes, such as viscous fingering [3], dielectric breakdown [4,5], etc. In spite of the apparent simplicity of the model, an analytic solution is still unavailable. Particularly, the exact value of the fractal dimension is not known. Some of the analytic approaches employed so far include the fixed-scale transformation (FST) [6], real-space renormalization group (RSRG) [7–9], and conformal mapping [10–13].

In DLA there is a seed cluster of particles fixed somewhere. A particle is released at a distance from the cluster, and performs a random walk until it attempts to penetrate the fixed cluster, in which case it sticks. Then the next particle is released, and so on. There are two common types of sticking conditions. The sticking condition described above is called ''bond DLA,'' because it occurs when the random walker attempts to cross a perimeter bond between an unoccupied site and the aggregate. In an earlier paper [14], we solved the bond-DLA problem using a Markovian process. Here we apply similar methods to the ''site-DLA'' case, where sticking occurs as soon as the random walker arrives at a site that is a nearest neighbor to the aggregate. Since it is believed that the large-scale structure of DLA is not sensitive to the type of sticking conditions used [15,6], one expects both problems to yield the same asymptotic fractal structures.

DLA can be grown in various geometries. In this paper, we deal with the cylindrical geometry in two dimensions (2D), where the particles are emitted from a distant horizontal line at the top, while the seed cluster is a parallel line at the bottom, with periodic boundary conditions on the sides. We only consider relatively narrow cylinders, with widths ranging from $N=2$ to $N=10$. Even though the analysis in this paper is solely 2D, the same techniques can be applied in higher dimensions.

An exact solution of bond DLA with $N=2$ was published in 1998 [16]. A generalization of the same approach was used in order to solve slightly wider cases with N between 3 and 7 [14]. The solution presented in the latter case is not exact, but still, it presents a well-controlled series of approximations in the sense that any desired numerical accuracy could be obtained, provided that a sufficiently high order of approximation is used. The difficulty with performing a high-order calculation is that its complexity grows exponentially.

The main idea in these references and in this paper is to follow the dynamics of the growing front. The shape of the interface determines the unique solution to the Laplace equation that determines the growth probabilities. The structure of the aggregate behind the interface is irrelevant and so is the history that led to the current interface. Each growth process changes the interface. We can therefore describe DLA as a Markovian flow in the space of interface configurations. The Markov states are the possible shapes of the interface, which are indexed by an integer, usually denoted by i or j. $P_i(t+1)$, the probability that the interface is in state i at time $t+1$, depends only on the state of the interface at time t. The conditional transition probabilities from state j to state i make up the evolution matrix $E_{i,j}$, which is time-independent. Thus, the dynamics of the Markov chain is described by the Master equations,

$$P_i(t+1)=\sum_j E_{i,j}P_j(t), \quad i=1,2,\ldots . \tag{1.1}$$

Each matrix element $E_{i,j}$ corresponds to a particular growth process, and the sum of j runs over all the interface configurations (whose number may be infinite). In order to fully describe the dynamics, it is necessary to calculate the probabilities of all the possible growth processes, for each of the possible initial configurations of the interface. We calculate the growth probabilities by solving the discrete Laplace equation on a lattice for a function Φ, which corresponds to the average density of random walkers,

$$\nabla^2\Phi=0. \tag{1.2}$$

In the dielectric breakdown model (DBM) [4,5], Φ has an electrostatic meaning, so it is also commonly referred to as the ''potential.''

Usually, the equation set (1.1) is infinite because the number of possible shapes the interface may assume is unlimited. This may pose a problem for two reasons. For one, it is difficult to include all of the possibilities systematically. The case of bond DLA with $N=2$ is a counterexample, where the complete set of possible configurations can be easily characterized using a single parameter. This is because the interface has the shape of a step whose height j can be any nonnegative integer [16]. For $N>2$, however, it is very difficult to parametrize the shape of the interface, even with the use of more than one parameter, because complex overhangs may occur [14]. The second problem is that even if it were possible to account for a complete infinite set of configurations, it would still be awkward to analyze the Markov process, e.g., finding its fixed point. Instead of accounting for all the configurations, we make an approximation by employing some consistent truncation scheme on the list of configurations. In the Oth-order approximation we include only the top O rows of a configuration and truncate the rest; the list of configurations is sorted according to the maximal height difference, Δm, between the lowest and highest particles on the interface [14]. In the Oth-order approximation, only a finite set of configurations with $\Delta m \leqslant O$ is taken into account. The configurations with $\Delta m > O$ are truncated so that only their top O rows are taken into account (below the Oth row all the sites are considered to be occupied). This truncation does not have a noticeable effect on the upward growth probability (the growth probability at the tip), because of the exponential decay of the potential inside deep fjords. Because of this exponential decay, the approximation converges very fast as a function of O. Unfortunately, the number of configurations diverges exponentially with O, so that the calculation can be carried out only for relatively low order (depending on the width N and on the strength of the computer).

In the case of site DLA, the situation is a bit simpler than in bond DLA, because it is generally harder for the random walker to penetrate deep into a fjord. A particle will only be able to enter fjords that are at least three sites wide, unlike the case of bond DLA, where a particle can go into a single-column fjord. This makes the solution of site DLA with $N=2$ and $N=3$ much simpler, because they both have only a finite number of interface configurations. The narrowest cylinder that can have an arbitrarily deep fjord (a configuration with an arbitrarily large Δm) arises for $N=4$, and thus there is an infinite number of configurations. However, there can be no fluctuations in the width of the fjord, so in this sense this case resembles the $N=2$ case in bond DLA. For $N>4$, the approximation method must be used, but generally, for the same N and O the number of configurations in site DLA is much smaller than in bond DLA, so it is possible to perform higher-order calculations for wider cylinders.

Once an order of approximation O is chosen, there is only a finite number of configurations, $N_c(N,O)$, which depends both on N and on O. The Markov process is then closed and irreducible. Closed means that $\Sigma_{i=1}^{N_c} E_{i,j}=1$ for $j=1,\ldots,N_c$, and irreducible means that there is a finite probability to go from any initial state j to any final state i during a finite number of time steps. A basic theorem in Markov theory states that a closed and irreducible process necessarily has a single fixed point [17]. This fixed point represents the steady-state probabilities for the various interface configurations in the asymptotic time limit. The theorem is also true for an infinite number of states, so one can conclude that the unapproximated process also converges to a steady state. As mentioned, this steady state is characterized, for example, by a time-independent average density ρ.

The fixed-point equations are

$$P_i^* = \sum_j E_{i,j} P_j^*, \quad i=1,2,\ldots . \tag{1.3}$$

This means that $\mathbf{P}^*$ is the normalized eigenvector of the evolution matrix $\mathbf{E}$ with an eigenvalue of 1. Once the steady state $\mathbf{P}^*$ is calculated, it is possible to evaluate the steady-state average upward growth probability,

$$\langle p_{\mathrm{up}} \rangle^* = \sum_{j=1}^{N_c} P_j^* p_{\mathrm{up}}(j), \tag{1.4}$$

where $p_{\mathrm{up}}(j)$ is the total upward growth probability for configuration j. The average steady-state density of the aggregate is then given by

$$\rho(N) = \frac{1}{N \langle p_{\mathrm{up}} \rangle^*}. \tag{1.5}$$

Here, the density is written explicitly as a function of N. By $\rho(N)$ we denote the true value of the density, in the limit $O \to \infty$. We denote the result of the Oth-order approximation by $\rho_c(N,O)$.

As mentioned, the number of configurations grows exponentially with O and N, so it becomes unfeasible to make the calculation for high values of O and N. We perform calculations for $N \leqslant 10$. The calculated densities and the number of configurations are presented in Sec. II. We find that in order to obtain a relative accuracy of about 10^{-4}, it is necessary to go up to $O=N-2$ or $O=N-1$. This is achieved for $N \leqslant 8$, but for $N=9,10$ it is too heavy a task for our computer resources. In spite of this, we are able to successfully extrapolate O to infinity for $N=9$ and $N=10$. The calculated densities are compared to direct measurements from cylindrical site-DLA simulations, and are found to be the same up to the accuracy of the simulation, which is about 0.01% or better.

The fractal dimension D is extracted from the assumption that $\rho(N) \propto N^{-(d-D)}$, where $d=2$ is the Euclidean dimension. In general, one should also expect some corrections to scaling, especially for low N's, i.e.,

$$\rho(N) = A N^{-(d-D)} (1 + B/N^{\theta} + \cdots), \tag{1.6}$$

where A and B are some constants, θ represents the leading correction exponent, and the dots stand for a series of higher powers of $1/N$. This scaling hypothesis is validated by both the analytic enumeration computation and by the simulations, which were conducted up to $N=128$. The best fit of such a model to the enumeration data results in an estimate of the fractal dimension of cylindrical DLA in 2D, D

$=1.68\pm0.01$. The same fit is also performed with the simulation data, yielding $D=1.671\pm0.001$. This is to be compared with the value $D\approx1.66$ often found in the literature [6].

The differences between bond DLA and site DLA are manifested in the boundary conditions for the Laplace equation, and in the way the growth probabilities are extracted from the potential Φ. The boundary conditions at the top are

$$\lim_{m\to\infty}\frac{\partial\Phi(m,n)}{\partial m}=1,\quad n=0,\ldots,N-1, \tag{1.7}$$

where $\hat{\mathbf{m}}$ is the vertical direction (the growth direction) and $\hat{\mathbf{n}}$ denotes the periodic lateral direction. This describes a uniform flux of incoming particles. In the original DBM papers [4,5], a uniform potential is used instead of a uniform gradient, but if the distant boundary is very far, then the differences between the solutions for the two cases are exponentially small [16]. The determination of the boundary conditions on the aggregate should be done with care. In the case of bond DLA, the potential is set to 0 on the aggregate itself, while in site DLA the potential should be set to 0 on nearest-neighbor sites, i.e., on sites where growth might occur. Also, the derivation of the growth probabilities from the potential in site DLA is done a bit differently than in bond DLA, as explained in the next section.

The Laplace equation with these boundary conditions can be solved exactly [16,14]. The idea is to divide the plane (or space in higher dimensions) into two parts. The upper part is an empty semi-infinite rectangle that begins at the row of the highest site on the lower boundary and continues upward *ad infinitum*. The lower part contains the aggregate and extends from the highest row downwards. The row that contains the highest particle in the aggregate is usually set as a reference row with $m=0$. Thus, in bond DLA, the upper part has $m\geqslant0$ and the lower part has $m\leqslant0$, and in site DLA, the upper part has $m\geqslant1$ and the lower part has $m\leqslant1$, as explained in more detail in Sec. II. Note that in either case the dividing row is considered to belong to both parts. In the upper part, it is possible to express the potentials in row $m+1$ as a linear combination of those in row m,

$$\Phi(m+1,n)=1+\sum_{n'=0}^{N-1}\Phi(m,n')g_N(n-n'). \tag{1.8}$$

This is especially useful for the bottom row of the upper part, $m=0$ or $m=1$ (depending on the type of sticking conditions). The boundary Green's function $g_N(n)$, appearing in Eq. (1.8), is given by

$$g_N(n)=\frac{1}{N}\sum_{l=0}^{N-1}e^{-\kappa_l}\cos(k_l n). \tag{1.9}$$

The finite set of allowed wave vectors $k_l=(2\pi/N)l$ for $l=0,\ldots,N-1$ is imposed by the horizontal periodicity. The factor κ_l is related to k_l through the dispersion relation

$$\sinh(\kappa/2)=\pm\sin(k/2), \tag{1.10}$$

or more explicitly,

$$e^{-\kappa(k)}=2-\cos(k)-\sqrt{[2-\cos(k)]^2-1}. \tag{1.11}$$

An interesting property of the Green's function is that

$$\sum_{n=0}^{N-1}g_N(n)=1. \tag{1.12}$$

This property was proved algebraically in Ref. [16] and was used in Refs. [16,14] to check the computations of the Green's function. It is also used in the sample calculation of Sec. II B in the current paper for the same purpose.

Usually, there is no general derivation for the solution in the lower part. In spite of that, the number of sites in the lower part is finite and not too large, so it is possible to simply write the equations for each of the potentials. The solution of the resulting finite and linear set of equations is then straightforward.

The paper is organized as follows. In Sec. II, we present in detail the differences in the computation of the growth probabilities between bond- and site-sticking conditions. This presentation also explains the connection with the Laplace equation more rigorously. After that we perform a few sample calculations, for $N=2$ and $N=3$, in order to demonstrate the method presented in the Introduction. We then report the results of the computations for N between 4 and 10 for various orders of approximations O. We point out that the results collapse onto a universal function that enables the extrapolation $O\to\infty$ for $N=8$, 9, and 10. This extrapolation reduces the error appreciably. In Sec. III, we present the simulation we made in order to verify our theoretical predictions. This presentation also explains how the boundary Green's function $g_N(n)$ is used in some way as a probability function, in order to make the simulation more efficient. We summarize in Sec. IV.

II. ENUMERATION

Our computation method is referred to as enumeration, because it involves a systematic processing of some complete lists of configurations.

A. The differences between site- and bond-sticking conditions

There are two differences between site- and bond-sticking conditions. The first is in the boundary conditions used for the solution of the Laplace equation, and the second is in the way the potentials are used to determine the growth probabilities. In order to explain this, it is important to understand the subtleties of the relation between DLA and the Laplace equation. In DLA, the random walker is injected into a random site near the remote boundary and it diffuses until it attempts to cross a perimeter bond, in which case it gets

stuck. A possible way of measuring the growth probabilities for a particular interface configuration is to send many random walkers, one after the other, and remove them after they stick. One has to keep track of how many particles get stuck in each site. Eventually, the growth probabilities per site are estimated by the fraction of particles that got stuck in each site. Instead of releasing the random walkers one at a time, it is more efficient to release many of them simultaneously, and let them perform a random walk without interacting with each other. Moreover, instead of releasing a large amount of particles in a single batch and waiting until all of them stick, it is also possible to inject them at a constant rate near the boundary, i.e., in each time step inject a new particle into each site near the boundary with a uniform probability r. The advantage in this way of performing the measurement is that after an initial equilibration time the system arrives at a steady state, which is characterized by a time-independent average number of random walkers in all of the sites, including sites that are not near any of the boundaries. In the steady state, the average number of random walkers entering into the system in each time step at the upper boundary is equal to the average number of random walkers vanishing out of the lower boundary. Denote the average number of random walkers in each site in the steady state by $\Phi(m,n)$; then it satisfies the discrete Laplace equation (1.2), because every random walker is equally likely to go to any one of its nearest neighbors and because Φ is time-independent.

Special care should be give to sites near the boundaries. Near the upper boundary, each site has only three nearest neighbors, and particles are added at a constant rate r, therefore,

$$\Phi(m,n)=\frac{1}{4}[\Phi(m,n-1)+\Phi(m,n+1)+\Phi(m-1,n)+\Phi(m,n)]+r. \tag{2.1}$$

Note that the last term on the left before r is $\Phi(m,n)$, instead of $\Phi(m+1,n)$, because the particles that randomly choose to go up are unable to do so because of the boundary, and therefore they remain in the same place. Now, let us define $\Phi(m+1,n)\equiv\Phi(m,n)+4r$ as a fictitious density above the boundary. Then we see that Eq. (2.1) turns into the standard Laplace equation. This shows that instead of using the injection rate parameter r, it is possible to use the regular Laplace equation with the Neumann-type boundary conditions that require the specification of the electric field, which corresponds to the difference in the potential across the upper boundary. Since the value of r does not change the growth probabilities, we are free to choose any value for it. If, for example, we choose $r=\frac{1}{4}$, then the boundary conditions at the top are

$$\frac{\partial\Phi}{\partial m}\equiv\Phi(m+1,n)-\Phi(m,n)=1 \tag{2.2}$$

for $n=0,1,\ldots,N-1$. We choose the upper boundary to be very far away from the lower one, because this simplifies the analytic expressions involved in the solution of the Laplace equation, while leaving the sticking probabilities practically unchanged.

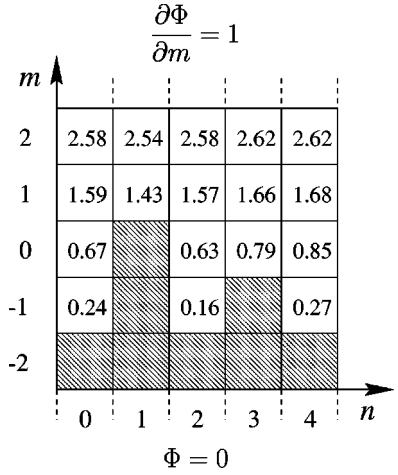

FIG. 1. An example of the solution of the Laplace equation $\nabla^2\Phi(m,n)=0$, with boundary conditions $\Phi=0$ on the aggregate and $\partial\Phi/\partial m=1$ on the upper distant boundary. Here, the width is $N=5$ and there are periodic boundary conditions on the sides. The axes indicate the directions of the coordinates m and n. These boundary conditions are consistent with bond-sticking conditions.

The difference between site and bond DLA appears in the bottom boundary conditions. In bond DLA, each random walker that attempts to go into the aggregate is taken out of the system. Thus the Laplace equation is valid for sites that are nearest neighbors to the aggregate, if we choose the boundary conditions $\Phi=0$ on the aggregate itself. In site DLA, random walkers are removed as soon as they arrive at sites that are nearest neighbors to the aggregate and therefore we impose $\Phi=0$ there instead. Figure 1 shows the solution to the Laplace equation around a particular aggregate for bond-sticking conditions, and Fig. 2 shows the solution near

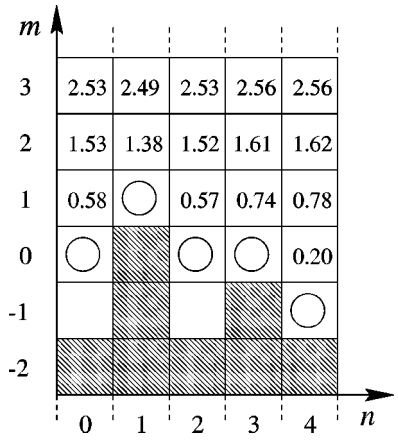

FIG. 2. The solution to the Laplace equation near the same aggregate as in Fig. 1, only with site-sticking conditions. The circles denote the perimeter sites where a random walker might stick. The boundary conditions are that $\Phi=0$ on these sites, unlike the case of bond-sticking conditions where $\Phi=0$ on the aggregate itself. The boundary conditions $\partial\Phi/\partial m=1$ at large m remain unchanged.

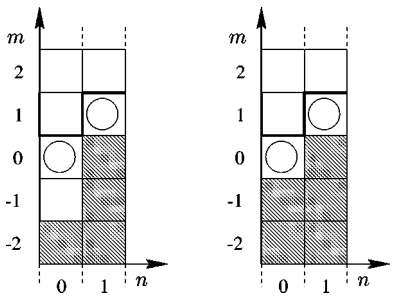

FIG. 3. Two different aggregates (represented by the dashed squares) with $N=2$, having exactly the same set of sites where a random walker may stick (shown in circles), and thus having the same boundary (the bold line) for the Laplace equation, where $\Phi=0$.

the same aggregate for site-sticking conditions. The figure also shows that the boundary for the Laplace equation is obtained by coating the aggregate with a layer of circled sites. This may cause two different aggregates to have the same boundary for the Laplace equation, see Fig. 3. Consequently, any two different aggregates that have the same boundary for the Laplace equation must have the exact same set of growth probabilities and can therefore be considered as equivalent. Thus, from now on when we refer to an interface configuration, we relate to the shape of the boundary for the Laplace equation. The probability to be in such a configuration is a sum over all the underlying aggregate configurations. Another effect of the transition to the Laplace boundary is the narrowing of fjords. The padding of the aggregate by circled sites causes all the fjords to be narrower by two sites. Thus, a random walker can only penetrate into aggregates that have branches that are at least three sites apart.

For both types of sticking conditions, the growth probability in each site is evaluated as the average number of random walkers that stick in that site per unit time, normalized by the total number of particles sticking during a single time step. In the steady state, the normalization factor is equal to the average total number of random walkers injected into the system, which is equal to $rN=N/4$.

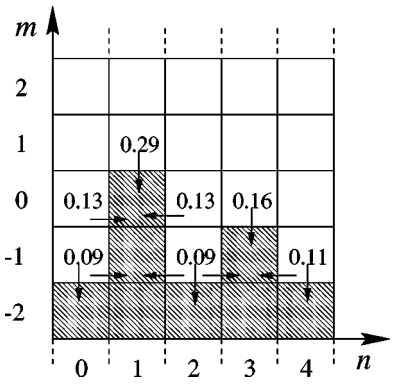

FIG. 4. The growth probabilities for the aggregate shown in Fig. 1. The growth probability in each perimeter site is proportional to the potential Φ at that site and to the number of bonds N_b leading from the site into the aggregate (denoted by arrows), e.g., $N_b=3$ for the site at $(-1,2)$ and $N_b=1$ for the site $(0,2)$ right above it.

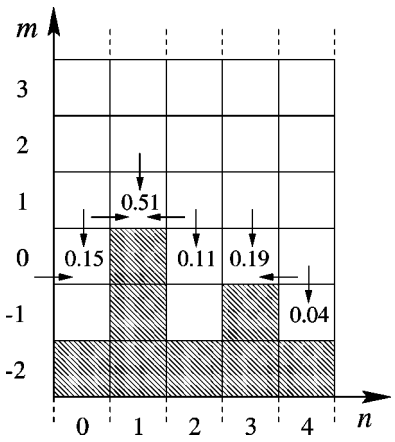

FIG. 5. The sticking probabilities in each of the circled sites of Fig. 2. They are computed by summing over all of the bonds that go into each site (denoted by arrows), unlike the case of bond-sticking conditions, where contributions are summed over bonds that go out of each site .

In bond DLA, a fraction of 1/4 of the particles vanishes after choosing to go via bonds that connect to the aggregate. The average total number of particles sticking in a site would then be a sum over all of its interface bonds, $\Sigma_b\Phi/4=N_b\Phi/4$, where N_b is the number of bonds that connect the site to the aggregate. Thus the growth probability in each site is $N_b\Phi/N$, see Fig. 4. In Ref. [14], we arrive at the same result using the discrete Gauss theorem.

In site DLA, we must sum over bonds that lead *into* the site, rather than out of it. The growth probability per site is therefore

$$p_{\text{site}}(m,n)=\frac{1}{N}\sum_{\text{nn}}\Phi(m',n'), \tag{2.3}$$

where $p_{\text{site}}(m,n)$ is the total sticking probability at the perimeter site (m,n), see Fig. 5. Unlike the case of bond-sticking conditions, where a single potential determines the sticking probability in a particular site, now the potentials in several different sites contribute. This difference gives the uppermost tip of the aggregate an even greater advantage relative to bond DLA, because a single-particle tip gathers contributions from three sides in site DLA, whereas in bond DLA the only contribution is from above. This comes in addition to the screening property of the Laplace equation (common to both types of sticking conditions), which causes the sticking probabilities at the lower parts of the interface to decrease exponentially.

B. Exact solutions for $N=2,3$

The best way to explain the enumeration method is to show some sample calculations in detail. We present here the two simplest cases, namely, $N=2$ and $N=3$. In these cases, there is only a finite number of configurations, so it is possible to get an exact solution with no need for approximations.

For $N=2$, the interface of the aggregate itself has an infinite number of possible configurations, because it has the

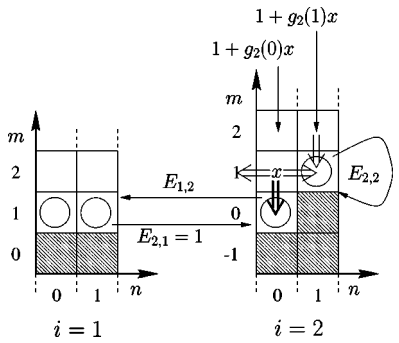

FIG. 6. The two possible configurations for $N=2$. The circles denote the sites where a random walker might stick. Also shown are the possible transitions between them, denoted by arrows, and the relevant matrix elements $E_{i,j}$. The distribution of the potential Φ over the lattice is demonstrated only for configuration $i=2$, see text for explanation. The double arrows ($\Downarrow$, $\Rightarrow$, and $\Leftarrow$) show the bonds of the possible access paths, which a random walker can take into the circled sites. The bold double arrow shows the only bond going into site (0,0). The other three bonds lead into site (1,1).

shape of a step whose height j can be any non-negative integer [16]. However, in site DLA there are only two distinct states: $j=0$ and $j>0$. The case $j=0$ refers to a flat interface, i.e., the two columns have the same height, and a growth process will create a step with $j=1$, with probability 1. For any step size $j>0$, there are only two sites where a random walker may stick: above the highest particle in the aggregate, or on its side; see Fig. 3. There is no possibility for the random walker to penetrate into a fjord in $N=2$, because it is too narrow, and the particle would stick at its entrance. The two configurations are indexed by $i=1$ and $i=2$, respectively, and are shown in Fig. 6.

We now begin building the evolution matrix **E** by finding the growth probabilities for each of the two configurations. As mentioned, configuration $i=1$ turns into $i=2$ with probability 1, hence $E_{1,1}=0$ and $E_{2,1}=1$. It is important to keep track of the total upward growth probability for each configuration, $p_{\mathrm{up}}(i)$, that corresponds to events in which a newly stuck particle is higher than all of the particles in the aggregate. In this case $p_{\mathrm{up}}(1)=1$.

In order to solve for $i=2$, we first have to compute the Green's function according to Eq. (1.9), which gives

$$g_2(0)=2-\sqrt{2}=0.5858,$$
$$g_2(1)=\sqrt{2}-1=0.4142. \tag{2.4}$$

We check our calculations by verifying that $g_2(0)+g_2(1)=1$, as expected from Eq. (1.12). The potential Φ near the growth sites can be expressed in terms of the variable $x\equiv\Phi(1,0)$ according to Eq. (1.8), as shown in Fig. 6. We usually set the row containing the highest particle in the aggregate as the reference row, with $m=0$. Thus, the row $m=1$ always contains the highest circled site that belongs to the Laplace boundary. Each of the sites in row $m=1$ contributes to the potentials in the sites in row $m=2$. The weight of the contribution is equal to the value of the Green's function $g_N(n)$, where n is the horizontal distance between the contributing site in row $m=1$ and the evaluated site in row $m=2$. In this simple case, there is only one site with a nonzero potential, namely, $\Phi(1,0)$, which is yet unknown, and which we denote by x. The site (1,1) on its side is nearest neighbor to the aggregate and therefore we set $\Phi(1,1)=0$. Thus, the potential of the sites in row $m=2$ only has a contribution from x. More specifically, $\Phi(2,0)=1+g_2(0)x$ because it is right above x, and $\Phi(2,1)=1+g_2(1)x$ because it is removed by one site. The potential $\Phi(2,0)$ does not contribute to any growth process, but is important for solving for x. The variable x is found using its Laplace equation,

$$4x=1+g_2(0)x,$$
$$\Rightarrow x=\frac{2-\sqrt{2}}{2}=0.2929. \tag{2.5}$$

Growth in site (0,0) results in the flat configuration $i=1$. It can only occur via one bond from site (1,0), denoted by a bold double arrow ($\Downarrow$) in Fig. 6. Hence,

$$E_{1,2}=\frac{x}{2}=\frac{2-\sqrt{2}}{4}=0.1464, \tag{2.6}$$

where the denominator comes from the normalization factor $N=2$. Growth can also occur in site (1,1). This time there are three different bonds coming from two sites: there are two bonds coming from (1,0) and an additional one coming from (2,1). This upward growth results in the same configuration, so

$$E_{2,2}=p_{\mathrm{up}}(2)=\frac{1}{2}[2x+1+g_2(1)x]=\frac{2+\sqrt{2}}{4}=0.8536. \tag{2.7}$$

This concludes the calculation of all of the growth processes. The resulting evolution matrix is

$$\mathbf{E}=\begin{bmatrix}0 & 0.1464\\ 1 & 0.8536\end{bmatrix}. \tag{2.8}$$

We verify that the matrix is properly normalized by noting that the sum of the terms in each of its columns is equal to 1, i.e.,

$$\sum_{i=1}^{2} E_{i,j}=1, \quad j=1,2. \tag{2.9}$$

The general theorem mentioned in the Introduction ensures the existence of a single eigenvector with an eigenvalue of 1, or in other words, a fixed point vector $\mathbf{P}^*$ that satisfies

$$\mathbf{P}^*=\mathbf{E}\mathbf{P}^*. \tag{2.10}$$

The fact that the process is closed is manifested in Eq. (2.9). The process is also irreducible because there is a finite probability to go from any initial state to any final state during a finite number of time steps. The fact that there is a single fixed point implies that starting from any initial state, the system will converge to the fixed point. This fixed point

represents the asymptotic time probabilities for seeing either one of the two possible configurations.

The eigenvalues are the roots of the characteristic polynomial,

$$\lambda_0 = 1, \qquad \lambda_1 = -\frac{2-\sqrt{2}}{4} = -0.1464, \tag{2.11}$$

and the normalized fixed-point vector $\mathbf{P}^*$ is given by

$$P_1^* = \frac{5-\sqrt{8}}{17} = 0.1277, \qquad P_2^* = \frac{12+\sqrt{8}}{17} = 0.8723. \tag{2.12}$$

The steady-state weights enable us to calculate the average upward growth probability,

$$\langle p_{\mathrm{up}} \rangle^* = \sum_{i=1}^{2} P_i^* p_{\mathrm{up}}(i) = \frac{12+\sqrt{8}}{17} = 0.8723, \tag{2.13}$$

which is connected to the mean density,

$$\rho(2) = \frac{1}{2\langle p_{\mathrm{up}} \rangle^*} = \frac{6-\sqrt{2}}{8} = 0.5732. \tag{2.14}$$

It is also possible to calculate the rate of convergence to the steady state. In general, the rate of convergence is determined by the largest eigenvalue of $\mathbf{E}$, other than 1. Suppose that at time $t=0$ the state of the system differs from the steady state $\mathbf{P}(0) \neq \mathbf{P}^*$. The difference vector

$$\mathbf{v}(0) \equiv \mathbf{P}(0) - \mathbf{P}^* \tag{2.15}$$

belongs to the linear subspace of vectors $V = \{\mathbf{v} | \Sigma v_i = 0\}$, because both $\mathbf{P}(0)$ and $\mathbf{P}^*$ are normalized probability vectors and thus the sum of their components is equal to 1. Now, Eq. (2.9) ensures that V is an eigensubspace of $\mathbf{E}$, and as such it must contain at least one eigenvector. Since in this simple case the space of configurations is only two-dimensional, then V is one-dimensional, and $\mathbf{v}(0)$ is necessarily an eigenvector with the eigenvalue $\lambda_1 = -0.1464$. After t time steps the state of the system is

$$\mathbf{P}(t) = \mathbf{E}^t \mathbf{P}(0) = \mathbf{P}^* + \lambda_1^t \mathbf{v}(0). \tag{2.16}$$

Therefore, the deviation from the steady state decays exponentially,

$$\mathbf{P}(t) - \mathbf{P}^* = \lambda_1^t \mathbf{v}(0) = (-1)^t e^{-t/\tau} \mathbf{v}(0), \tag{2.17}$$

where

$$\tau \equiv -\frac{1}{\ln|\lambda_1|} = 0.5584. \tag{2.18}$$

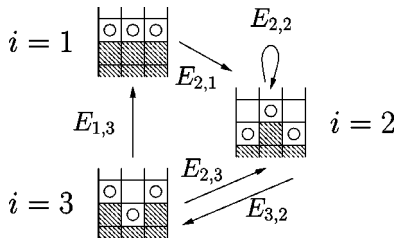

FIG. 7. The possible configurations and the possible transitions between them for $N=3$.

This means that a single time step is practically sufficient to arrive at the steady state. All of these theoretical predictions agree with results obtained from numeric simulations, up to the accuracy of the simulation, which is better than 10^{-5}. This dynamics is actually exactly the same as the first-order approximation of the frustrated climber model in Ref. [14], except that the analysis of the temporal convergence is a little bit more refined there.

The solution of the case $N=3$ is also relatively simple, because again there is only a finite number of growth configurations. This is because the width of the widest possible fjord is two sites, which is still insufficient for a random walker to penetrate, i.e., a random walker sticks as soon as it enters into a fjord. The three possible configurations are indexed in Fig. 7. These are the same as the three configurations of the first-order approximation for bond DLA with $N=3$ [14]. As in the example of $N=2$, we proceed to calculate the probabilities for every growth process in each of the configurations. Once again, we first calculate the Green's function,

$$g_3(0) = \frac{6-\sqrt{21}}{3} = 0.4725, \qquad g_3(1) = g_3(2) = \frac{1-g_3(0)}{2} = \frac{\sqrt{21}-3}{6} = 0.2638. \tag{2.19}$$

The first configuration, $i=1$, grows with probability 1 into configuration $i=2$. Thus, $E_{2,1}=1$ and $E_{1,1}=E_{3,1}=0$, and also $p_{\mathrm{up}}(1)=1$. The potential diagram for $i=2$ is shown in Fig. 8. Because of symmetry it is possible to conclude that $\Phi(1,0)=\Phi(1,2)=x$. The Laplace equation for x is

$$4x = x + 1 + [g_3(0) + g_3(1)]x, \qquad \Rightarrow x = \frac{9-\sqrt{21}}{10} = 0.4417. \tag{2.20}$$

The sticking probability at (0,0) is $x/3$, because there is a single connecting bond, and because the normalization factor is 1/3 for this case. The resulting configuration is $i=3$, however a sticking event at (0,2) also leads to $i=3$, so that $E_{3,2} = \frac{2}{3}x = (9-\sqrt{21})/15 = 0.2945$. The other possibility is an upward growth at (2,1), which results in the initial configuration $i=2$. Thus, $E_{2,2} = p_{\mathrm{up}}(2) = 1 - E_{3,2} = (6+\sqrt{21})/15 = 0.7055$ and $E_{1,2}=0$.

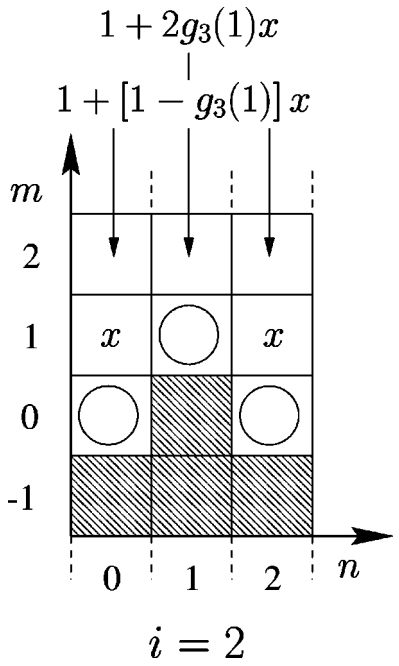

FIG. 8. A ''potential diagram'': the potentials $\Phi(m,n)$ of configuration $i=2$, expressed in terms of the variable x.

The potential diagram for $i=3$ is shown in Fig. 9. The Laplace equation is

$$4x = 1 + g_3(0)x, \qquad \Rightarrow x = \frac{6-\sqrt{21}}{5} = 0.2835. \tag{2.21}$$

A sticking event in (0,1) leads to $i=1$, therefore $E_{1,3}=x/3$. The other possible sticking events at (1,0) or (1,2) involve upward growths, which result in $i=2$, i.e., $E_{2,3}=p_{\mathrm{up}}(3)=1-x/3=(9+\sqrt{21})/15=0.9055$. This completes the calculation of all the elements of the evolution matrix:

$$\mathbf{E} = \begin{bmatrix} 0 & 0 & 0.0945 \\ 1 & 0.7055 & 0.9055 \\ 0 & 0.2945 & 0 \end{bmatrix}. \tag{2.22}$$

The normalized fixed point of the matrix is

$$\mathbf{P}^* = [0.0210, \quad 0.7562, \quad 0.2227]. \tag{2.23}$$

This enables the computation of the average upward growth probability and of the average density:

$$\langle p_{\mathrm{up}} \rangle^* = \sum_{j=1}^{3} P_j^* p_{\mathrm{up}}(j) = 0.756\,245, \qquad \rho = \frac{1}{3\langle p_{\mathrm{up}} \rangle^*} = 0.440\,774. \tag{2.24}$$

The second largest eigenvalue determines the characteristic time constant of the exponential convergence to the steady state,

$$\tau = -\frac{1}{\ln|\lambda_1|} = 0.56. \tag{2.25}$$

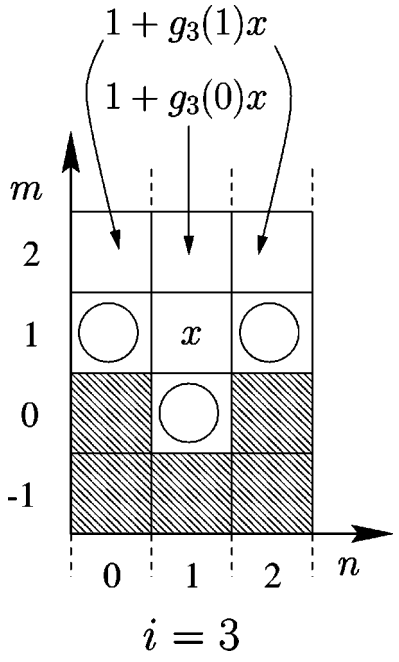

FIG. 9. The potential diagram for configuration $i=3$.

C. Approximations for $N>3$

The two examples of the previous sections, for $N=2$ and $N=3$, are special because there is only a finite number of possible configurations. The case $N=4$ is the narrowest cylinder that can have a fjord that is three sites wide. Since this fjord can be arbitrarily deep, there is an infinite number of configurations. In spite of that, every configuration that has a fjord that is more than one site deep is uniquely determined by its depth, i.e., there is only one configuration with $\Delta m=2$, a single configuration with $\Delta m=3$, and in general a single configuration with a specific Δm if $\Delta m \geqslant 2$. The unique configuration with $\Delta m=2$ is shown in Fig. 10, along with the single configuration with a specific Δm that is larger than 2. Other than that, there are four possible configurations with $\Delta m=1$, which are shown in Fig. 11, and finally the trivial flat configuration with $\Delta m=0$.

This case resembles bond DLA with $N=2$ [16], in the sense that in both cases there is an infinite number of configurations, but this infinity can be represented using a single parameter. In Ref. [16], this parameter is called ''the step size'' and is denoted by j, but actually it is the same as Δm. The case of site DLA with $N=4$ is a bit different, because there are four configurations with $\Delta m=1$ instead of one. There is also a resemblance to the solution of the Laplace equation for the two cases, because in both cases the Laplace equation is solved on a single column with zero boundary conditions on the sides. Thus, in both cases there is an ex-

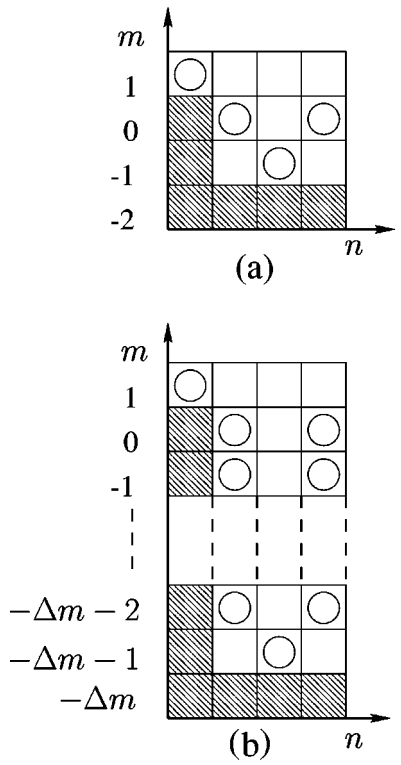

FIG. 10. The only configurations for a cylinder of width $N=4$: (a) $\Delta m=2$, (b) $\Delta m>2$.

ponential decay of the potential inside the fjord, which is governed by the multiplicative factor $e^{-\kappa_f}=2-\sqrt{3}$. This enables us to treat the current case in an analogous way to the previous one. This could have given us analytic expressions for the Markovian matrix $E_{i,j}$, $i,j=1,2,\ldots,\infty$, for the steady-state vector P_i^*, $i=1,2,\ldots,\infty$, and for the distribution of gaps inside the aggregate. However, we omit the presentation of this calculation because it is not the main interest of this work, and so we treat the case of $N=4$ in the same way as $N>4$.

For $N>4$, the boundary may be complex, and it cannot be easily characterized because the width of a fjord can fluctuate and overhangs may appear. We therefore use the approximation scheme described in the Introduction, which was also used for bond DLA [14]. The calculation procedure involves

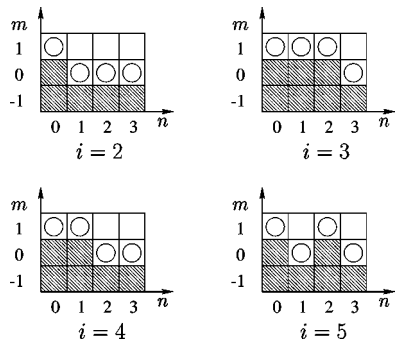

FIG. 11. The four possible configurations for $N=4$ with $\Delta m=1$. These configurations are indexed between $i=2$ and $i=5$, and the flat configuration with $\Delta m=0$ is indexed by $i=1$.

going over all the possible configurations to some order, and calculating their set of growth probabilities. It is feasible to perform this task manually when the number of configurations is relatively small, but as N and O increase, the number of configurations grows exponentially and it becomes impractical to do so. We use the same computer program that was used for bond-sticking conditions, after making the necessary adjustments due to the site-sticking conditions. Manual calculations may still be important as test cases to check the operation of the program.

The program goes over all of the possible configurations systematically. It starts with the trivial flat configuration ($\Delta m=0$), which is indexed by $j=1$. This configuration has only one possible growth process, which occurs with probability 1, that turns the interface into configuration $j=2$, which has a single bump. The program then continues to $j=2$ and analyzes its growth probabilities. Every growth process changes the shape of the boundary. Each time a particle sticks in a certain site, the program has to identify the newly formed configuration. In order to do so, it marks all of the nearest neighbors of the newly attached particle, because new particles may stick there. The new configuration is searched for in the existing list of configurations, which were already analyzed by the program. If it does not exist, then it is added at the end of the list. In either case, the program identifies the index of the resultant configuration *i*. Now, if the index of the original configuration is *j*, then the growth probability is stored in the matrix element $E_{i,j}$.

A configuration is characterized using the set of sites that are connected to infinity because these are the sites that are accessible to the random walker. Of course, any site that is higher than the highest site on the boundary is connected to infinity. Hence, it is sufficient to specify only the set of sites that are not higher than the highest boundary site (the region $m\leqslant 1$). A single growth process may cause a whole region of sites to disconnect from infinity, for instance by sealing off an entrance to a fjord. This means that it is not sufficient to mark the nearest neighbors of a newly attached particle, but that it is necessary to recheck the complete set of sites that are connected to infinity. We perform this by an algorithm that marks this set recursively.

Special care has to be taken for upward growth processes, because they may cause Δm to exceed O. In case this happens, the bottom row of the configuration is truncated. Finally, symmetry has to be taken into account. Rotations around the axis of the cylinder and reflections about any vertical axis do not change the growth probabilities or the steady-state weights, so the set of all of the symmetric configurations is represented by a single canonical choice. More specifically, a configuration is represented by a binary word that consists of $N\times O$ digits that correspond to the sites; the empty sites that are on the exterior are given a value of 1, and the rest of the sites are assigned with zeros. We choose the canonical form as the word that has the maximal numerical value.

After the complete list of configurations is processed, the calculation of the evolution matrix is completed, and it is closed, i.e., $\Sigma_i E_{i,j}=1$ for every j. Then the steady-state vector $\mathbf{P}^*$ is calculated iteratively by applying the evolution ma-

TABLE I. The approximated densities ρ_c and the number of configurations N_c for various orders O and cylinder widths N. The approximated densities from enumeration are compared to simulation results. In addition, the extrapolated density $\rho(N,O\to\infty)$ is also presented.

$N\backslash O$	Simulation	$O\to\infty$	1	2	3	4	5	6	7	8
2	0.5732		0.5732							
			2							
3	0.4408		0.4408							
			3							
4	0.3744	0.3744	0.3743	0.3750	0.3744	0.3744	0.3744	0.3744		
			5	6	7	8	9	10		
5	0.3334	0.3334	0.3323	0.3355	0.3336	0.3334	0.3334	0.3334	0.3334	
			7	10	14	24	52	134	378	
6	0.3049	0.3049	0.3025	0.3094	0.3057	0.3050	0.3049	0.3049	0.3049	0.3049
			12	21	35	94	395	1970	10344	55161
7	0.2837	0.2837	0.2798	0.2908	0.2857	0.2840	0.2837	0.2837	0.2837	
			17	38	76	280	1831	13575	98479	
8	0.2671	0.2671	0.2616	0.2767	0.2707	0.2679	0.2672	0.2671		
			29	81	190	846	7605	83043		
9	0.2536	0.2537	0.2467	0.2655	0.2593	0.2551	0.2540			
			45	161	451	2421	29220			
10	0.2424	0.2426	0.2341	0.2562	0.2503	0.2450	0.2431			
			77	349	1152	7213	111067			
11	0.2329		0.2233	0.2483	0.2431	0.2368				
			125	733	2885	21688				
12	0.2247		0.2139	0.2415	0.2371	0.2300				
			223	1627	7504	67450				

trix many times on some initial-state vector. This method is much faster than any of the standard techniques for solving a set of linear equations, especially when the number of variables is very large. The next step is to calculate the average upward growth probability, according to Eq. (1.4), and the average density, according to Eq. (1.5). Our computer resources enabled us to conduct the enumeration only up to a finite order $O_{\max}$ that depends on N. As explained above, for $N=2$ and $N=3$ there exists a finite number of configurations, and higher-order approximations are irrelevant. One may be surprised that we are able to reach $O=8$ for $N=6$, but we do not reach such a high order for $N=4$ and $N=5$, because there are definitely fewer configurations in the same order of approximation for lower N's. The reason for this is that very good convergence is achieved already for $O=N$, so we had little to gain by going to much higher orders, and we stop at $O=N+2$ for $N=4$ and $N=5$. The calculated densities $\rho_c(N,O)$ are presented in Table I, together with the number of configurations N_c. The table also presents the extrapolation and simulation results.

D. The extrapolation of the order of approximation to infinity, $O\to\infty$

Very good accuracy (about 10^{-4}) is also obtained for $N=8$, even though $O_{\max}=N-2=6$. However, for $N\geqslant 9$ the results are not very accurate, because the maximal available order is only $O=5$ for $N=9,10$ and $O=4$ for $N=11,12$. In spite of that, we are able to arrive at a more precise estimation for $N=9,10$ by extrapolating $O\to\infty$. The extrapolation does not improve the accuracy of the cases $N=11,12$ to a satisfactory level. Our aim is to deduce the value of $\rho(N)=\lim_{O\to\infty}\rho_c(N,O)$ from the limited range of available values for O. We start by noting that our data practically reached asymptotia for $N=4,5,6$. We detect that the differences, $\rho_c(O,N)-\rho_c(O+1,N)$, decay exponentially and thus conclude that the function $f=\ln[\rho_c(N,O)/\rho(N)-1]$ is very close to being linear. Substituting the parametrization $f=\beta-\alpha O/N$, we are able to extract the three unknowns—α, β, and $\rho(N)$—using at least three data points. For $N=6$ and $O=4$, 5, and 6, we find that $\beta=0.03$ and $\alpha=12.31$. The value of $\rho(6)$ turns out to be very close to the highest available approximation $\rho_c(6,8)$.

Scaling theory would imply that, for large N and O, f should become a universal function, which depends only on the scaled ratio $x=O/N$ (without an additional dependence on N). Following this expectation, we thus conjecture the general relation

$$\rho_c(N,O)=\rho(N)[1+e^{f(O/N)}], \tag{2.26}$$

with $f(x)\simeq -12.3x$ for $N,O\gg 1$.

To test this conjecture, we estimated $\rho(N)$ for $N\geqslant 4$ via

$$\rho(N)\simeq\frac{\rho_c(N,O_{\max})}{1+e^{f(O_{\max}/N)}}. \tag{2.27}$$

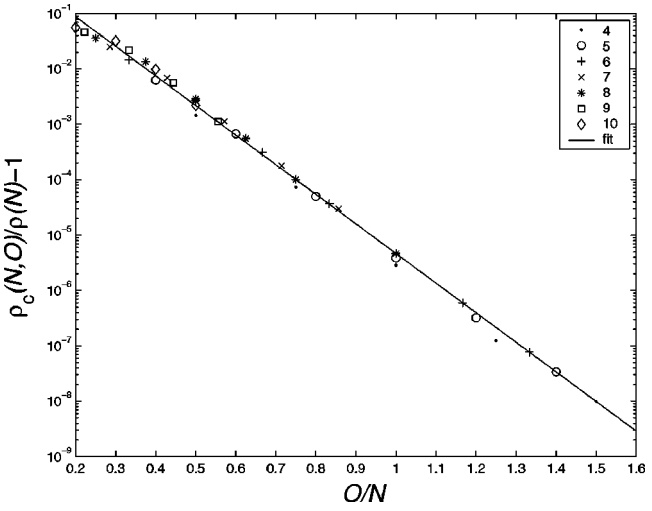

FIG. 12. Data collapse of $e^f=[\rho_c(N,O)/\rho(N)-1]$ vs O/N for all the data points with $4\leqslant N\leqslant 10$ and $O>2$, on a semilogarithmic scale. The continuous line shows the linear approximation $f \simeq -12.3O/N$.

We have then used this estimate to calculate $\rho_c(N,O)/\rho(N)$ for $O<O_{\max}$. The resulting values are shown in Fig. 12, together with the line $f(x)=-12.3x$. Clearly, all the values for $O/N\gtrsim 0.4$ are consistent with our conjectured form for $f(x)$.

The values of $\rho(N)$, as deduced using Eq. (2.27), are listed in Table I. Clearly, they all agree with the values from the simulations, except for small deviations that appear for $N=9$ and 10. In the cases $N=11,12$ the deviations are relatively large, because $O_{\max}$ is too small, and hence the extrapolation results are not specified.

E. An enumeration-based estimate of the fractal dimension *D*

In the preceding section, we obtain very accurate estimates of the asymptotic ($O\to\infty$) average steady-state densities $\rho(N)$. In this section, we extrapolate the latter densities in the limit $N\to\infty$ in order to find the fractal dimension D. Consider an N^d segment in the steady-state regime of growth. Assuming that the structure is a self-similar fractal, which has no characteristic length scale other than N, we expect that the average mass of the segment would be proportional to N^D, and that the density would be proportional to N^{D-d}. In principle, however, one expects some corrections to scaling as in Eq. (1.6). Taking only the first correction term of that equation into account, we get an approximation that depends on the four parameters D, A, B, and θ:

$$\rho_a(N)=AN^{D-d}\left(1+\frac{B}{N^\theta}\right), \tag{2.28}$$

where the subscript a denotes that this is an approximation. Using the four data points with $7\leqslant N\leqslant 10$, a fit to Eq. (2.28) yields $D=1.64$, $\ln(A)=-0.63$, $B=1.31$, and $\theta=1.48$. The calculation of the parameters can also be based on more than the minimal four points, using a least mean-square error method. We choose to minimize the logarithmic (or relative) errors $\Delta\rho/\rho$ rather than the errors in the densities $\Delta\rho$, because we find them to be more uniformly distributed. The results of the fit using the six data points with $5\leqslant N\leqslant 10$ yield $D=1.74\pm 0.06$, $\ln(A)=-1.0\pm 0.3$, $B=1.5\pm 0.6$, and $\theta=0.80\pm 0.13$. The error estimates are evaluated using a confidence level of 0.95. Since the fit yields a value for θ that is close to 1, we also try a three-parameter fit, fixing $\theta=1$. Using the three rightmost data points for $N=8$, 9, and 10 gives $D=1.68$, $\ln(A)=-0.799$, and $B=1.16$. Using more points with $5\leqslant N\leqslant 10$, we get

$$\begin{aligned} D&=1.68\pm 0.01,\\ \ln(A)&=-0.784\pm 0.016,\\ B&=1.12\pm 0.05. \end{aligned} \tag{2.29}$$

Finally, an alternative four-parameter form, including only ''analytic'' corrections, is

$$\rho_a(N)=AN^{D-d}\left(1+\frac{B}{N}+\frac{C}{N^2}\right). \tag{2.30}$$

This time the results for $7\leqslant N\leqslant 10$ are $D=1.65$, $\ln(A)=-0.68$, $B=0.55$, and $C=1.10$, and the least mean-square calculation for $5\leqslant N\leqslant 10$ yields $D=1.70\pm 0.02$, $\ln(A)=-0.87\pm 0.08$, $B=1.5\pm 0.4$, and $C=-0.5\pm 0.4$.

We thus conclude that the fractal dimension of cylindrical DLA is $D\simeq 1.68\pm 0.01$, close to the results of earlier numerical work [6].

III. SIMULATION

As mentioned, our analytical enumeration results are confirmed by simulations. In this section, we describe how our simulations were conducted, paying special attention to the boundary Green's function $g_N(n)$, which is given a new probabilistic meaning. We also discuss the accuracy of the results, and finally, we try to fit the results to some approximations as in the end of the preceding section and obtain some more estimates of the fractal dimension.

Our simulation is performed on a lattice, which is represented by a 2D array variable. Each of the variables in the array can assume one of two possible values, 1 or 0, that determine whether the relevant site is occupied by an aggregate particle or not, respectively. The size of the array is $(14N)\times N$, i.e., its width is N and it is composed of 14 blocks of $N\times N$ sites stacked one on top of the other. The number 14 is quite arbitrary and could be chosen differently. In principle, the lattice should be tall enough to allow the aggregate to arrive at a steady state, and also to allow a margin at the top, because the average density of the aggregate is lower near the growing front. Each time a new cluster is initialized, the lattice array is cleared so that all of its variables are set to 0, except for the bottom row, which is set to 1. This means that the initial shape of the aggregate is a horizontal line at the bottom of the lattice. A random walker is characterized by the coordinates (m,n) of its position. In each simulation step, a direction is chosen randomly and the

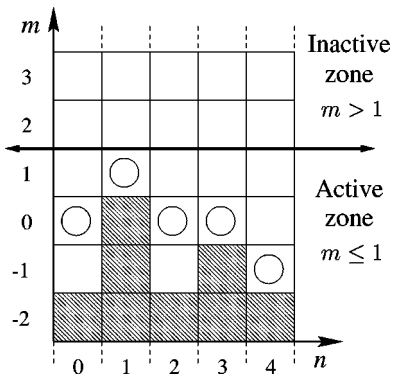

FIG. 13. The bold line separates between the upper inactive zone with $m>1$ and the lower zone with $m\leqslant 1$. A random walker cannot stick in the inactive zone.

particle is advanced in that direction. If the particle happens to go into a site that is nearest neighbor to the aggregate, then it sticks, i.e., the value of the relevant lattice variable is updated from 0 to 1. Then the next random walker is released, and so on.

A. The role of the Green's function

In principle, each new random walker should be released far above the aggregate, near the upper distant boundary. In practice, nothing can happen to the random walker (it cannot stick) until it crosses the bold line in Fig. 13. This line is drawn between the highest row where a random walker can stick ($m=1$) and the row above it ($m=2$), and thus it differentiates between the active zone below the line, with $m \leqslant 1$, and the inactive zone above it, with $m>1$. The projection of the path of the random walker on the vertical axis (its m coordinate) is also a random walk, only in one dimension (1D). Usually in 1D there is a probability of 1/2 to go up and the same probability to go down, but in our case, there is a probability of 1/4 to go in either direction, and a probability of 1/2 to stay at the same row. Nevertheless, this motion is still equivalent to a random walk, however the effective time step is longer. A quality of 1D random walks is that there is a probability of 1 to arrive at any site (no matter how far) within a finite time. Therefore, there is a probability 1 that eventually the random walker would cross the line from the inactive zone into the active zone. The random walker is equally likely to cross this line at any of the N sites, so instead of waiting for a long time, it is more efficient to start the simulation by inserting the random walker in a random site just below the line in the active zone [18].

But what happens if the path of the random walker happens to cross the line into the inactive zone? Once more we apply the same reasoning and claim that ultimately the random walker would recross the line downwards at some point with probability 1. Unlike the initial insertion, this time the distribution of the reentry point is not uniform. It is quite easy to see, for example, that there is a greater chance for the particle to reenter at the exact same site from which it exited than for it to reenter at a site that is far away. Let us denote by $\Psi(m,n;n')$ the probability that if the particle is at some initial site (m,n) in the inactive zone $(m>1)$, then it will cross the line for the first time at $(m'=1,n')$. In the next time step, the random walker moves to one of its nearest neighbors with equal probability. Therefore, $\Psi(m,n;n')$ must be equal to the average of Ψ on all the nearest neighbors. This implies that Ψ satisfies the Laplace equation (in the coordinates m and n),

$$\nabla^2\Psi(m,n;n')=0. \tag{3.1}$$

The boundary conditions for Ψ at the lower boundary are

$$\Psi(m=1,n;n')=\begin{cases}1, & n=n'\\ 0 & \text{otherwise.}\end{cases} \tag{3.2}$$

This is true because if the random walker is already in the row $m'=1$, then it already passed the line between $m=1$ and $m=2$ and so it stops before it starts. The boundary conditions at the top are $\Psi=\text{const}$, or equivalently,

$$\lim_{m\to\infty}\frac{\partial\Psi}{\partial m}=0. \tag{3.3}$$

These are the exact same conditions satisfied by the Green's function [16], and so the theorem about the uniqueness of the solution of the Laplace equation with the boundary condition assures that Ψ is equal to the Green function, and especially at the first row above the line $m=1$,

$$\Psi(1,n;n')=g_N(n-n'). \tag{3.4}$$

This means that each time the random walker attempts to cross the line to the inactive zone, it can be returned to the active zone immediately. The distance of the reentry point from the exit point should be chosen randomly from the distribution defined by the Green's function $g_N(n)$. This policy saves a lot of simulation time in comparison with the alternative option of letting the random walker wander freely until it finally sticks, or until it passes some arbitrary critical distance from the aggregate. We note in passing that the discussion in this section proves Eq. (1.12) in an alternative, probabilistic approach, simply due to the fact that $g_N(n)$ is a probability function.

B. Analyzing the statistics

Figure 14 shows an example of a typical *density profile*, which is the average density as a function of height. Only the middle section of the aggregate is taken into account in measuring the average steady-state density $\rho(N)$. Our impression is that a margin of N sites from each side is enough, but we work with margins of $2N$. A possible way of estimating the accuracy of this average is by taking the standard deviation and normalizing by the square root of the number of rows that participate in the averaging. This is somewhat optimistic, however, and would produce very low error estimates, because this calculation assumes statistical independence between adjacent rows, where in fact there are significant correlations. The right factor to normalize by is therefore the

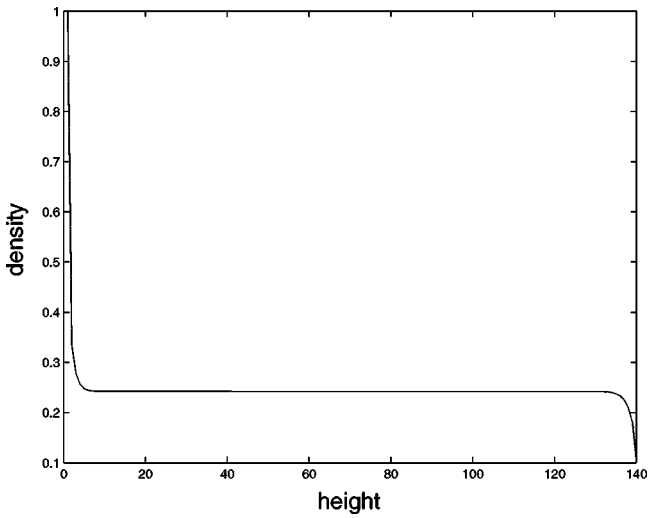

FIG. 14. The density profile as a function of height for a lattice with $N=10$ averaged over some $N_i \approx 2\times 10^7$ iterations. The height of the lattice is 140 sites.

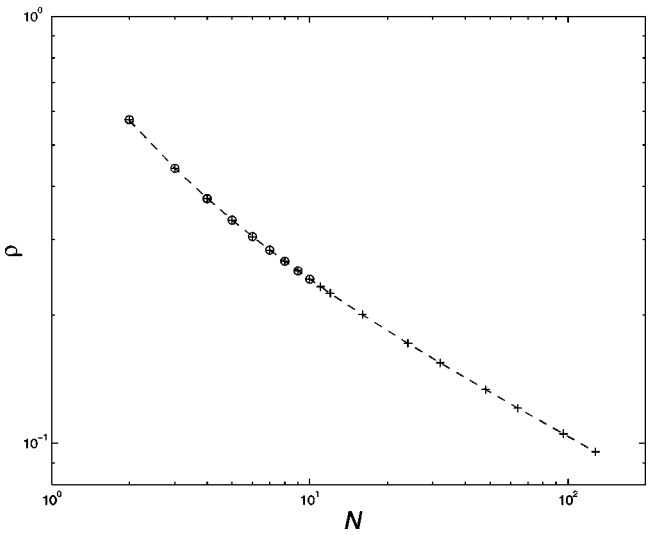

FIG. 15. A plot of $\rho(N)$ vs N on log-log scales. The plus signs denote the simulation results, the dashed line denotes $\rho_a(N)$, the best fit to the three-parameter approximation of Eq. (2.28), with $\theta=1$. The circles denote the enumeration results.

square root of the effective number of independent rows. Since the aggregate is fractal, the only available length scale is N, and therefore the correlation length ξ should be proportional to N. We therefore conservatively guess that two rows that are N rows apart are independent, and hence we estimate the accuracy by the standard deviation divided by $\sqrt{10}$, because there are 10 blocks of $N\times N$ is the steady-state region in our simulations. This error estimate is expected to have the correct dependence on the number of $N\times N$ blocks, but there could be some numerical factor missing.

An alternative way of measuring $\rho(N)$ is by measuring $\langle p_{\rm up}\rangle^*$ directly and using Eq. (1.5). After the aggregate reaches a height of $2N$, we assume that it is in the steady state and we start gathering statistics. In particular, we count the number of upward growth events, when the random walker sticks above all the particles in the aggregate. Our results show very good correspondence between the two different methods; the typical relative difference is on the order of 10^{-6}.

The simulations were carried out for the following values of N: 2,3, . . . ,12, 16, 24, 32, 48, 64, 96, and 128. We did not go beyond that because our computer resources did not suffice to iterate a large enough number of clusters to obtain a relative accuracy of about 10^{-4} or better, as obtained for the other cases.

We now proceed to fit the results for the 10 available data points with $128\geqslant N\geqslant 10$ in a similar way to Sec. II E. The difference is that now we use the error estimates σ_i to give weights to the different data points, because not all the accuracies are the same. This way the fit will allow greater residuals for data points with larger error estimates. Our first attempt is to fit the four-parameter approximation of Eq. (2.28). The results are $D=1.673\pm 0.002$, $\ln(A)=-0.770\pm 0.0013$, $B=1.03\pm 0.06$, and $\theta=0.96\pm 0.06$. The maximal relative residual is 1.2×10^{-4}. Once more we set $\theta=1$ and perform the fit for the remaining three parameters. The results are

$$D=1.671\pm 0.001,$$

$$\ln(A)=-0.762\pm 0.003, \tag{3.5}$$

$$B=1.071\pm 0.015.$$

The resulting error estimates seem a bit too optimistic, perhaps also because of the presence of some systematic errors that are not taken into account. The simulation results are shown in Fig. 15 on log-log scales as plus signs, along with the latter three-parameter fit, shown as a dashed line. The figure also shows the enumeration results as circles. Since the differences are hardly noticeable, we display the relative (logarithmic) residuals $v_i\equiv[\rho(N_i)-\rho_a(N_i)]/\rho(N_i)$ separately in Fig. 16 on semilogarithmic scales, in comparison with the relative error estimates $\pm\sigma_i$. The maximal relative residual is 1.3×10^{-4}. This is consistent with the order of magnitude of the estimated *a priori* errors.

A factor that indicates the compatibility between the *a priori* error estimates σ_i and the *a posteriori* residuals v_i is

$$\chi^2\equiv\frac{1}{N_d}\sum_i\left(\frac{v_i}{\sigma_i}\right)^2, \tag{3.6}$$

where N_d, the number of degrees of freedom, is equal to the number of data points minus the number of unknown parameters. The value of χ^2 should be close to 1. In the latter fit, we get $\chi^2=0.9$, whereas we get $\chi^2=0.3$ in the former. The results of the fit imply that the three-parameter approximation is sound.

For the sake of comparison, we also try to fit to the other test approximations that were introduced in the preceding section. The best fit to the four-parameter approximation in Eq. (2.30) is $D=1.6721\pm 0.0012$, $\ln(A)=-0.766\pm 0.006$, $B=1.12\pm 0.07$, and $C=-0.28\pm 0.4$. In this approximation, the residuals are not lowered drastically; the maximal rela-

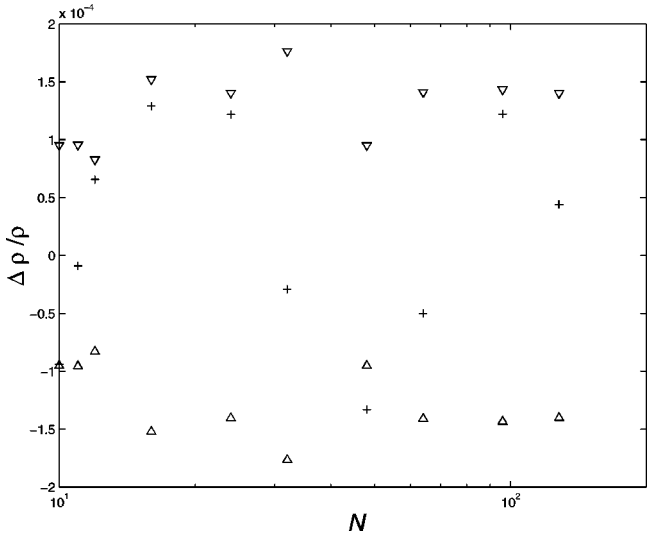

FIG. 16. The relative residuals $v=(\rho-\rho_a)/\rho$ (the plus signs) vs N on semilogarithmic scales. The upper and lower triangles show the estimated confidence intervals (errors) of the simulation data, $\pm\sigma$.

tive residual is 1.1×10^{-4} and $\chi^2=0.2$. The error estimate of the fourth parameter C is much greater than the error estimates of the other parameters. The contribution of the term with the C parameter is on the same order of magnitude as the residuals, at least for the data points with large N's. This implies that there may be significant contributions from the noise (the errors), and therefore its inclusion is redundant.

IV. SUMMARY

In this paper, we continue our endeavor to solve cylindrical DLA analytically, i.e., to calculate the steady-state average density ρ as a function of the cylinder width N, and to find the fractal dimension D. Unlike our previous work, which deals with bond-sticking conditions [14], this work solves for site-sticking conditions. The immediate problem in following our Markovian method is that, except for $N=2,3$, there is usually an infinite number of configurations. The case $N=4$ has an infinite number of configurations, but is still relatively simple. The large variety of possible complex interface shapes for $N\geqslant5$ prevents the inclusion of all the configurations and compels the use of an approximation scheme, in which only a finite number of rows O of the growing front near the tip are included. This approximation works because of the exponential decay of the Laplace potential Φ inside deep fjords. The approximation leaves a finite number of configurations to work with, and thus the computational procedure can be completed.

We find that this is a well-controlled approximation, in the sense that any desired numerical accuracy can be achieved provided that a high enough order of approximation O is used. The results are summarized in Table I, which shows the computed density ρ_c for various values of N and O along with the number of relevant configurations N_c. An evident fact is that N_c grows very rapidly as a function of O and N, making it impractical to perform the calculation for wide cylinders. We note that in order to obtain the same relative accuracy, it is necessary to use $O\propto N$, e.g., in order to obtain a relative accuracy better than 10^{-4} one should use at least $O=N-1$. This is the case for $N\leqslant7$, where the results are very accurate, but not so for $N\geqslant8$, where our available computer resources allowed only lower-order computations. As discussed in Sec. II D, we are able to improve the estimates in these cases by extrapolating $O\to\infty$, taking advantage of the universal exponential decay of $\rho_c(N,O)/\rho(N)$ with the scaled variable O/N. Table I also compares the enumeration estimates with direct measurements from simulations, and finds them to agree within the simulation errors. Once accurate estimates are obtained for $\rho(N)$ for $N\leqslant10$, they are fitted to a power-law approximation with a correction to a scaling term according to Eq. (2.28). The fit (with $\theta=1$) gives an estimate of the fractal dimension $D=1.68\pm0.01$.

Besides the range $2\leqslant N\leqslant10$, simulations are also performed on cylinders with larger N's in the range $10\leqslant N\leqslant128$. The relative errors of the measurements of $\rho(N)$ are estimated around 10^{-4}. The simulation data are also fitted to the same approximations. Once again, the three-parameter approximation proves most appropriate and the resulting fractal dimension this time is $D=1.671\pm0.001$. The fact that the enumeration and simulation-based estimates of the fractal dimension are very close is a good indication of their accuracy.

The last statement should be taken with some caution in light of evidence that raises doubts concerning self-similarity in radial DLA [19–21], or suggesting some very slow crossovers [22,23]. Indeed, radial DLA is somewhat different from cylindrical DLA, as manifested by the difference between their fractal dimensions: $D=1.71$ for radial DLA [24,25] and $D=1.66$ for cylindrical DLA (this difference is still not fully understood).

We also tried performing the exact calculations for $N=11$ and 12, but managed to go only up to $O_{\max}=4$. This was insufficient for extrapolation with an accuracy that is comparable to the rest of the data points. With the aid of stronger computers, we think that it would be possible and beneficial to compute a few more data points $\rho(N)$, which would help to obtain more accurate estimates of the fractal dimension. Also, the techniques discussed here could be used to find the fractal dimension of cylindrical DLA in 3D. However, since a much larger number of configurations can be expected, this task would also probably require the aid of a very strong computer.

There are a few differences between site DLA and bond DLA. The boundary conditions for the Laplace equation are a little bit different; in bond DLA, the potential is set to zero on the aggregate itself, whereas in site DLA, the potential is set to zero on sites that are nearest neighbors of the aggregate. Also, the growth probabilities are computed somewhat differently: in bond DLA, contributions are summed over bonds that go out of a site where sticking may occur, whereas they are summed over bonds that go into it in site DLA. The normalization factor, however, is equal to the width N in both cases. In the case of site-sticking conditions, there is an effective thickening of branches and thus a nar-

rowing of fjords. Thus, there is a notable decrease in the probability of a random walker to penetrate deep into fjords. This also causes the number of configurations for a particular choice of N and O to be considerably less for site DLA in comparison with bond DLA. Therefore, accurate enumeration results can be obtained for larger N's and O's in site DLA. The extrapolation $O \to \infty$ performed in this paper was not done in Ref. [14], which deals with bond DLA, because the technique was not developed at that time. When we apply the method to the bond-DLA case, we manage to improve the relative accuracy of the highest available approximations, $\rho_c(N, O_{\max}(N))$ for $N=6,7$, by an order of magnitude: from about 1.2×10^{-3} to 2×10^{-4} for $N=6$ and from 5×10^{-2} to 1.6×10^{-3} for $N=7$. This extrapolation is based on the data points for $N=5$. The relative accuracy of $\rho_c(N, O_{\max}(N))$ for $N\leqslant5$ is better than 10^{-4} and hence the extrapolation is not necessary. The estimate of the fractal dimension for site DLA, $D=1.68$, is to be compared with the bond-DLA enumeration result $D=1.64$ [14]. In contrast, the difference in the simulation results for the two cases is smaller: $D=1.67$ for site DLA and $D=1.66$ for bond DLA. Given the uncertainties, our results are consistent with universality with respect to the sticking conditions [15,6].

ACKNOWLEDGMENTS

We thank Peter Jones, Brooks Harris, Yonathan Shapir, Torstein Jøssang, Barbara Drossel, and Leonid Levitov for helpful discussions. We also thank Yiftah Navot for helping with the computer program by suggesting more efficient data structures and algorithms. This work was supported by a grant from the German-Israeli Foundation (GIF).

[1] T. A. Witten and L. M. Sander, Phys. Rev. B **27**, 5686 (1983).
[2] B. Mandelbrot, *The Fractal Geometry of Nature* (Freeman, New York, 1982).
[3] J. Feder, *Fractals* (Plenum Press, New York, 1988).
[4] L. Niemeyer, L. Pietronero, and H. J. Wiesmann, Phys. Rev. Lett. **52**, 1033 (1984).
[5] L. Pietronero and H. J. Wiesmann, J. Stat. Phys. **36**, 909 (1984).
[6] A. Erzan, L. Pietronero, and A. Vespignani, Rev. Mod. Phys. **67**, 545 (1995).
[7] H. Gould, F. Family, and H. E. Stanley, Phys. Rev. Lett. **50**, 686 (1986).
[8] T. Nagatani, Phys. Rev. A **37**, 3514 (1988); **38**, 2632 (1988).
[9] X. R. Wang, Y. Shapir, and M. Rubinstein, Phys. Rev. A **39**, 5974 (1989); J. Phys. A **22**, L507 (1989).
[10] M. B. Hastings and L. S. Levitov, Physica D **116**, 244 (1998).
[11] M. B. Hastings, Phys. Rev. E **55**, 135 (1997).
[12] B. Davidovitch, H. G. E. Hentschel, Z. Olami, I. Procaccia, L. M.Sander;, and E. Somfai, Phys. Rev. E **59**, 1368 (1999).
[13] B. Davidovitch, M. J. Feigenbaum, H. G. E. Hentschel, and I. Procaccia, Phys. Rev. E **62**, 1706 (2000).
[14] B. Kol and A. Aharony, Phys. Rev. E **62**, 2531 (2000).
[15] R. Cafiero, L. Pietronero, and A. Vespignani, Phys. Rev. Lett. **70**, 3939 (1993).
[16] B. Kol and A. Aharony, Phys. Rev. E **58**, 4716 (1998).
[17] J. R. Norris, *Markov Chains* (Cambridge University Press, Cambridge, 1997).
[18] H. Kaufman, A. Vespignani, B. B. Mandelbrot, and L. Woog, Phys. Rev. E **52**, 5602 (1995).
[19] B. B. Mandelbrot, Physica A **191**, 95 (1992).
[20] B. B. Mandelbrot, H. Kaufman, A. Vespignani, I. Yekutieli, and C. H. Lam, Europhys. Lett. **29**, 599 (1995).
[21] B. B. Mandelbrot, A. Vespignani, and H. Kaufman, Europhys. Lett. **32**, 199 (1995).
[22] E. Somfai, L. M. Sander, and R. C. Ball, Phys. Rev. Lett. **83**, 5523 (1999).
[23] B. B. Mandelbrot, H. Kaufman, B. Kol, and A. Aharony (unpublished).
[24] S. Tolman and P. Meakin, Phys. Rev. A **40**, 428 (1989).
[25] P. Ossadnik, Physica A **176**, 454 (1991).